# Extraction of the Vibrational Dynamics from Spectra of Highly Excited Polyatomics: DCO

**Christof Jung**

*Centro de Ciencias Fisicas UNAM, Apartado Postal 48-3, 62251 Cuernavaca, Mexico*

**Howard S. Taylor* and Erdinç Atılgan**

*Department of Chemistry, University of Southern California, Los Angeles, California 90089*

*Received: October 31, 2001; In Final Form: January 23, 2002*

The effective spectroscopic Hamiltonian fitted to experiment by Troellsch and Temps (*Z. Phys. Chem.* **2001**, *215*, 207) and describing high vibrational excitation to bound and resonant states is used in conjunction with methods of nonlinear classical dynamics and semiclassical mechanics to extract, for all of the observed highly excited resonance levels in polyad 8, the molecular motions upon which they are quantized. Two types of interlaced dynamically distinct ladders of states are revealed. The rungs of these ladders intersperse, making the spectra complex. The resonant 2:2:1 frequency ratio of the DC and CO stretches and the bend, respectively, is what causes the complexity and is what caused past attempts at interpretation to be at best incomplete. All states are assigned with physically meaningful quantum numbers corresponding to quasiconserved quantities. Most interestingly, it is pointed out that much of the information and assignment can be done without any calculations at all, using only the qualitative ideas from nonlinear, semiclassical, and quantum mechanics, along with the information supplied by the experimentalist.

## 1. Introduction

The vibrationaly excited bound and resonant states of deuterated formyl radical, DCO, have been studied both experimentally[1,2] and theoretically.[1−4] The vibrational level structure of the molecule was found to be decomposable into distinctive polyads arising from a 1:1:2 resonance between the CD stretching, the CO stretching, and the DCO bending vibrations, respectively. As such, as energy increases various resonance couplings come into play, causing some of the local modes to disappear only to be replaced by new internal motions. Thus, ref 1 states that "only a minority of vibrational states can be unambiguously assigned". Reference 3, a theoretical effort using an excellent potential surface and state-of-the-art computational techniques, reported a "pleasing agreement between calculated and measured energy levels for bound states and for energies and widths for resonances". Despite this agreement, the paper[3] reports that a "strong 1:1:2 stretch−stretch−bend resonance prohibits unique assignment for the majority of vibrational states".

In ref 1, the spectrum was fit to a spectroscopic Hamiltonian that we will use and that we will describe in the next section. Also in ref 1, a whole array of analytic tools were applied to analyze the spectrum. Energies, widths (obtained after the addition of an absorbing potential to the spectroscopic Hamiltonian), and wave functions were computed in reasonable agreement with ref 3 (except, for reasons explained in the paper,[1] for those states with all excitation in the DC mode). Wave packets were propagated to obtain IVR rates and pathways, and a rationale was given for the 2-order-of-magnitude difference between the experimental state-specific decay constants and the statistical unimolecular rate theory prediction observed by Stöck et al.[2] Even with this effort, no assignment, in the sense of associating the states with three quantum numbers representing quasiconserved quantities, was able to be given, nor was any picture of the internal motions offered, especially for higher energies. We do agree with ref 1, as will be seen below, that the motion is between regular and statistical. We would say that a mixed phase space exists for higher energies.

The latest work on DCO (i.e., ref 4) uses the potential surface used in refs 2 and 3 and, in three dimensions, seeks and finds the periodic orbits that organize phase space. Certain states are shown to be associated with these said periodic orbits. This work makes no new assignments using those made in ref 1, the comments about which we have quoted above. Reference 4 shows that the wave functions for some series of states correlate with the normal-mode periodic orbits and a saddle-node periodic orbit. Only 2 of 45 states in polyad 8 are associated with periodic orbits, and most states in polyad 8 are not discussed.

Here, as in our previous work, we show that the bottleneck complications in wave function and phase space structure visualization and comparison, a result of working in 3D, can be avoided for DCO when an algebraic spectroscopic Hamiltonian is employed along with the polyad constant of motion.[5,6] The polyad constant of the motion, which measures the total level of excitation, commutes with the spectroscopic Hamiltonian, always exist when frequencies are in resonance, and does not have an analogue for Hamiltonians represented in terms of kinetic plus potential energy, is used to reduce the configurational dimension of both the classical and quantum problem to two. In 2D, working polyad by polyad, now much simpler wave functions can be compared to organizing structures obtained by mapping a much simpler (albeit still not very simple) phase space. As shown in our previous works,[7−10] where the limitations and reasons for the success of the method are discussed in detail, a comparison of these reduced but semiclassicaly exact 2D wave functions on the tori and periodic orbits of the 2D classical analysis yields a complete dynamics-based assignment in which the quantum numbers are quasiconstants of the motion.

10.1021/jp014008m CCC: $22.00 
Published on Web 03/07/2002

The increase of the quantum numbers represents an increase in excitation level of a given classical, qualitatively describable, internal motion. It will be seen that, most often, several different classes of such motions exist in the polyad at any one energy. Consequently, the level series or ladders based on such motions run in energy simultaneously. The experiment or a theory that is not based on classical organizing structures only sees the interleaving of all of the rungs of these ladders and cannot separate them. They see a "complex" spectrum that even seems to be uninterpretable and unassignable. Moreover, if polyads are not separated for experimental or theoretical reasons, further interleaving makes the situation appear worse. Here, we will show that, in polyad 8, two basic ladders coexist that can be associated with the basic elements of the spectroscopic Hamiltonian. These will be a 2:1 Fermi-resonant motion coupling the DC stretch and the bend with CO mode uncoupled and one in which the stretch−stretch coupling causes the local stretches to frequency lock, with both bonds generally increasing in length in sync. More details will be given below. In a sense, because these motions "might" be expected from the spectroscopic Hamiltonian (but then why not expect a Fermi resonance between CO stretch and the bend?), an achievement of this paper is to sort the levels into the simple ladders.

Section 2 of this paper discusses the spectroscopic Hamiltonian and the methodology used to achieve a reduced-dimension phase space. Section 3 gives the classical study of the phase space associated with polyad 8 and shows the association of the trivially obtained quantum wave functions with the organizing structures from which come the assignment, the ladders, and the description of the internal motions. Section 4 presents the conclusions, where it is pointed out that, once one has a generic knowledge of the classical nonlinear methodology and the phase space topology expected in such molecules, in this problem (and in CHBrClF[9] and $N_2O$[10] analysis), much of the information desired by the chemical physicist, spectroscopist, and theorist could have been obtained without any classical trajectory calculation and, in fact, without any calculations at all.

## 2. The Model and Its Reduction

As a model to describe the vibrations of DCO, use is made of the parametrized spectroscopic Hamiltonian set up in ref 1. Here, we adopt the parameter values given as fit III in Table I therein. It is a description in the three local modes $m$, $n$, and $b$ referring to the DC stretch, the CO stretch, and the bend, respectively. In ref 1, the model is defined by giving the Hamiltonian matrix in the separable basis of the number representation. The corresponding Hamiltonian operator in terms of harmonic raising and lowering operators is

$$H = \omega_m(a_m^\dagger a_m + a_m a_m^\dagger)/2 + \omega_n(a_n^\dagger a_n + a_n a_n^\dagger)/2 + \omega_b(a_b^\dagger a_b + a_b a_b^\dagger)/2 +$$

(linear local-mode terms, diagonal)

$$x_{mm}(a_m^\dagger a_m + a_m a_m^\dagger)^2/4 + x_{nn}(a_n^\dagger a_n + a_n a_n^\dagger)^2/4 + x_{bb}(a_b^\dagger a_b + a_b a_b^\dagger)^2/4 + x_{mn}(a_m^\dagger a_m + a_m a_m^\dagger)(a_n^\dagger a_n + a_n a_n^\dagger)/4 + x_{mb}(a_m^\dagger a_m + a_m a_m^\dagger)(a_b^\dagger a_b + a_b a_b^\dagger)/4 + x_{nb}(a_n^\dagger a_n + a_n a_n^\dagger)(a_b^\dagger a_b + a_b a_b^\dagger)/4 +$$

(quadratic anharmonicities, diagonal)

$$\lambda_1 a_m^\dagger a_n[1 + \lambda_1' a_m a_m^\dagger + \lambda_1'' a_n^\dagger a_n + \lambda_1'''(a_b^\dagger a_b + a_b a_b^\dagger)/2]/2 + \text{cc} +$$

(1:1 coupling between the two stretches, nondiagonal)

$$\lambda_2 {a_n}^2 {a_m^\dagger}^2 + \text{cc} +$$

(2:2 coupling between the two stretches, nondiagonal)

$$k_{mbb} a_m^\dagger {a_b}^2/(2\sqrt{2}) + \text{cc} +$$

($m-b$ Fermi resonance, nondiagonal)

$$k_{nbb} a_n^\dagger {a_b}^2 + \text{cc} \quad (1)$$

($n-b$ Fermi resonance, nondiagonal)

We have written all operator products in symmetric form for easier transition to the classical version, because in this order, we can use the Heisenberg correspondence relation

$$a_j^\dagger \rightarrow {I_j}^{1/2} \exp(i\phi_j), \quad a_j \rightarrow {I_j}^{1/2} \exp(-i\phi_j) \quad (2)$$

where $I_j$ and $\phi_j$ are actions and angles, respectively, of the corresponding degrees of freedom. This correspondence gives the classical Hamiltonian

$$H = \omega_m I_m + \omega_n I_n + \omega_b I_b + x_{mm}{I_m}^2 + x_{nn}{I_n}^2 + x_{bb}{I_b}^2 + x_{mn} I_m I_n + x_{mb} I_m I_b + x_{nb} I_n I_b + \lambda_1\sqrt{I_m I_n}(1 + \lambda_1' I_m + \lambda_1'' I_n + \lambda_1''' I_b)\cos(\phi_m - \phi_n) + \lambda_2 I_n I_m \cos(2\phi_m - 2\phi_n) + k_{mbb}\sqrt{I_m} I_b \cos(\phi_m - 2\phi_b)/\sqrt{2} + k_{nbb}\sqrt{I_n} I_b \cos(\phi_n - 2\phi_b)/\sqrt{2} - E_0 \quad (3)$$

In quantum mechanics, energies of states are usually measured relative to the lowest state. To have coincidence between classical and quantum energy, we subtract the constant $E_0$ from the classical Hamiltonian, which is the energy of $H$ for all elementary actions set to the value $^1/_2$. In the following, we call the angle-independent part $H_0$ and call the angle-dependent part the resonant interactions. As a conserved quantity, the quantum mechanical Hamiltonian has the polyad operator, which commutes with $H$

$$P = a_m^\dagger a_m + a_n^\dagger a_n + a_b^\dagger a_b/2 \quad (4)$$

The classical Hamiltonian has the corresponding conserved quantity

$$P = I_m + I_n + I_b/2 - {}^5/_4 \quad (5)$$

Here, we have subtracted the classical zero point to have the same numerical values for the quantum and classical polyad number. Next, we use the existence of this conserved quantity to reduce the system to one with two degrees of freedom. To make the reduction explicit, we apply a canonical transformation where $K = P + {}^5/_4$ is one of the new actions and where its conjugate angle $\theta$ becomes a cyclic variable. As the other two new actions $J_m$ and $J_n$, we use the old actions $I_m$ and $I_n$ to have a simple interpretation of the new actions. As the new angles $\psi_m$ and $\psi_n$ conjugate to $J_m$ and $J_n$, respectively, we construct slow variables such that the average speed of one of the new angles or some combination of them becomes zero whenever some frequency locking between the original degrees of freedom occurs. This will be extremely helpful in detecting the transition of the system from the original local modes to some new types

of motion as such transitions are always caused by some kind of frequency locking between the old modes. The following choice of the canonical transformation turned out to be useful

$$\begin{array}{ll} K = I_m + I_n + I_b/2 & \theta = 2\phi_b \\ J_m = I_m & \psi_m = \phi_m - 2\phi_b \\ J_n = I_n & \psi_n = \phi_n - 2\phi_b \end{array} \quad (6)$$

In the new coordinates, the Hamiltonian is

$$\begin{aligned} H = {} & \omega_m J_m + \omega_n J_n + \omega_b 2(K - J_m - J_n) + \\ & x_{mm} {J_m}^2 + x_{nn} {J_n}^2 + x_{bb} 4(K - J_m - J_n)^2 + x_{mn} J_m J_n + \\ & x_{mb} J_m 2(K - J_m - J_n) + x_{nb} J_n 2(K - J_m - J_n) + \\ & \lambda_1 \sqrt{J_m J_n}[1 + \lambda_1' J_m + \lambda_1'' J_n + \lambda_1''' (K - J_m - J_n)] \times \\ & \cos(\psi_m - \psi_n) + \lambda_2 J_m J_n \cos(2\psi_m - 2\psi_n) + \\ & k_{mbb} \sqrt{J_m} 2(K - J_m - J_n) \cos(\psi_m)/\sqrt{2} + \\ & k_{nbb} \sqrt{J_n} 2(K - J_m - J_n) \cos(\psi_n)/\sqrt{2} - E_0 \end{aligned} \quad (7)$$

The important structures in classical phase space will be visualized in Poincare sections. Important periodic orbits and general trajectories will be plotted in the reduced configuration space, which is the two-dimensional torus in the coordinates $\psi_m$ and $\psi_n$. A mercator-type representation of this torus (square-shaped representations of density and phase plots in our drawings) will be used for obvious reasons. The reader should remember that opposite points on the boundary of this projection are to be identified with each other. For comparison, the wave functions also have to be plotted in the same reduced configuration space. This is done by representing the number state basis function $|n_m, n_n, n_b>$ as the periodic plane wave

$$\begin{aligned} \exp[i(n_m\phi_m + n_n\phi_n + n_b\phi_b)] = {} & \\ \exp(iP\theta) \exp[i(n_m\psi_m + n_n\psi_n)] & \end{aligned} \quad (8)$$

on the configuration torus.[7,11] Thereby, the decomposition of a wave function into number basis states is translated into the Fourier decomposition of the corresponding function on the torus. Note that the expansion of a given eigenstate into number basis states contains contributions only from a single value of $P$. Therefore, the $\theta$ dependence of the whole eigenstate is only the common front factor $\exp(iP\theta)$, which is a pure phase and can be disregarded. As such, the eigenstate is represented as a function of the two angle variables $\psi_m$ and $\psi_n$. The expansion coefficients are those obtained from the diagonalization of the algebraic Hamiltonian, which is available from the fitting procedure.

This representation is semiclassical because Schrödinger quantization

($I \rightarrow -i\hbar\, \partial/\partial\psi$, $\psi \rightarrow \psi$) of general canonical coordinates is only semiclassical and, in addition, the order of the action- and angle-containing factors is not specified. Statements about which of the many schemes for ordering we use are appropriate and are made in ref 7.

Finally, we desire to relate trajectories in the reduced space with the motion of the atoms in the molecule. This is done by a lift procedure: Integration of $d\theta/dt = \partial H/\partial K$ gives $\theta(t)$, and undoing the canonical transformation gives all $I_j(t)$ and $\phi_j(t)$. Use of the harmonic expression relating $I$ and $\phi$ to $p^{\text{local}}$ and $q^{\text{local}}$, i.e.

$$I_k^{1/2} \exp(-i\phi_k) = (q_k + ip_k)/\sqrt{2}$$

$$I_k^{1/2} \exp(i\phi_k) = (q_k - ip_k)/\sqrt{2} \quad (9)$$

provides the motion of the atoms in harmonic local-mode displacements. We expect that these displacements are qualitatively similar to the true displacements of the atoms in position space.

A knowledge of the symmetries of the system in the reduced angle variables are helpful for the classical analysis and ultimately the quantum assignment. They are as follows:

(A) The original system is invariant under the translation

$$\phi_m \rightarrow \phi_m + 2\pi \quad (10)$$

This induces the invariance under the translation

$$\psi_m \rightarrow \psi_m + 2\pi \quad (11)$$

of the reduced Hamiltonian in new variables.

(B) The original system is invariant under the translation

$$\phi_n \rightarrow \phi_n + 2\pi \quad (12)$$

This induces the invariance under the translation

$$\psi_n \rightarrow \psi_n + 2\pi \quad (13)$$

in the new variables.

(C) The original system is invariant under the translation

$$\phi_b \rightarrow \phi_b + 2\pi \quad (14)$$

This does not lead to important consequences for the reduced system.

(D) All angles appear only as linear homogeneous expressions in the arguments of cosine functions. Therefore, the Hamiltonian is invariant under a simultaneous inversion of the angles. In the old variables, this symmetry is

$$(\phi_m, \phi_n, \phi_b) \rightarrow (-\phi_m, -\phi_n, -\phi_b) \quad (15)$$

In new angles, it is

$$(\psi_m, \psi_n) \rightarrow (-\psi_m, -\psi_n) \quad (16)$$

This implies that, to any given solution in terms of the action angle variables $\psi_m(s)$, $\psi_n(s)$, $J_m(s)$, $J_n(s)$ of Hamilton's equations of motion, the curve $-\psi_m(-s)$, $-\psi_n(-s)$, $J_m(-s)$, $J_n(-s)$ is also a solution of the equations of motion i.e., symmetry D is time reversal. Therefore, most orbits come in symmetry-related pairs. Common exceptions are such orbits as coincide exactly with their symmetry images. The combination of all of these symmetries will lead to corresponding symmetries in Poincare plots and in plots of wave functions.

### 3. Dynamics and Implications for Wave Functions

In this section, we describe the important structures in classical phase space and relate them to corresponding sequences of quantum states. As an example, we discuss all details for polyad $P = 8$ as we sweep the energy through this polyad. For other polyads, the dynamics is qualitatively the same as long as the polyad number is restricted to reasonable values. For each important form of motion, we show a classical Poincare map, the trajectories of the most important classical skeleton elements and the lifted motion in displacement space at a value of energy where some corresponding quantum state exists. For purposes

of comparison to the classical skeletal elements, in Figure 1a, we show the density and phase plots of all 45 quantum states of polyad 8.

**3.1. Class A.** At very low excitation, mode *m* starts as the fastest mode, but because of its enormous negative anharmonicity, the states with most of the excitation in mode *m* are the energetically lowest states within the polyads starting from polyad 4.

If the total Hamiltonian consisted only of $H_0$, then the surfaces of constant action would form an invariant foliation of the phase space. If the effective frequencies of the various modes are far from resonance, the interaction terms in the full Hamiltonian have moderate effect only and cause secondary KAM islands and chaotic layers only on sizes too small to be of importance for semiclassics. In such a case, most of the volume of phase space is still occupied by invariant KAM tori that are continuous deformations of the invariant surfaces of $H_0$. We will call these tori the primary tori. In this sense, the dynamics is dominated by the primary torus structure. Because of the deformation of the primary tori, the speed of the trajectories on them varies considerably, and as a consequence, the classical average density of the projections of these trajectories into configuration space varies strongly too. This will be transferred into a nonconstant density in configuration space of the corresponding quantum states that are carried by the primary torus structure via EBK quantization (Einstein−Brillouin−Keller method, see ref 12). Because the primary tori are continuous deformations of the invariant leaves of the unperturbed Hamiltonian $H_0$, we expect these corresponding quantum states to be continuous deformations of basis states, which are the eigenstates of $H_0$ (see eq 8). In our model of DCO, this happens at the lower end of the polyads for $P > 4$.

As an example, we show in Figure 2 the classical dynamics for $P = 8$ at energy 11800 which is the energy of quantum state 9 of polyad 8. Part a shows a Poincare plot in surface $\psi_m = 0$ with negative orientation. The KAM torus shown by the heavy line carries quantum state 9 according to the EBK method. The action integral along the line shown in Figure 2a has the value $^3/_2$. The action integral along a path in $\psi_m$ direction has a value of $^{11}/_2$. Remembering that the original degrees of freedom are oscillations and that, accordingly, the zero-point actions are $^1/_2$, we see that this state has quantum numbers 5 in the *m* direction and 1 in the *n* direction. Because the new actions $J_k$ conjugate to the new angles $\psi_k$ coincide with the old actions $I_k$, this state has five excitations in local mode *m* and one excitation in mode *n*. Because $P = 8$, it must have four excitations in mode *b*. In Figure 2b, we show a segment of a trajectory on this quantizing torus; in the long run, this trajectory fills the whole torus densely. Figure 2c−e shows the corresponding lifted motion projected into the three two-dimensional coordinate planes of the three-dimensional displacement space. We do not see any locking phenomenon. All three original modes of vibration move independently. In this sense, the motion is a continuously distorted local-mode motion. In the same way, we can classify many more states carried by primary tori according to the EBK method. All such states are classified into class A. Table 1 shows which states of the whole polyad belong to class A and which are obtained by EBK quantization of primary tori. These states can also be classified alternatively by an inspection of the wave function. For all states of class A, the phase function is a continuous deformation of a basis function and the excitation numbers in the *m* and *n* directions can be read off by counting the total phase advance along loops in the $\psi_m$ and $\psi_n$ directions, respectively, divided by $2\pi$. The magnitudes of states of class A wave functions do not show any nodal pattern. The wave function inspection method also works in some cases where the primary torus structure is already too destroyed for the EBK method to be applied but where the phase function can still be identified as a continuous deformation of a basis function. In Table 1, we indicate the states for which the EBK method works and those for which it does not. Figure 1a indicates which wave functions are in class A. The reader should note the generally "striped" pattern in the phase and can count the phase advances in the $\psi_m$ and $\psi_n$ direction to verify the assignment in Table 1.

**3.2. Class B.** For increasing energy, the effective frequencies of the modes come closer into resonance, and accordingly, the interaction terms in the Hamiltonian have more effect, the primary torus structure becomes destroyed in large parts of phase space and chaos starts to appear on a large scale. For $P = 8$, this effect sets in for energies around 12500, even though parts of the primary torus structure survive to higher energies, giving the coexistence of the influence of several important phase space structures at one value of the energy. This coincides with the energy at which some quantum states each simultaneously adopt a topographic structure different from class A in the intensity plots (Figure 1a) but might retain a similarity to class A in the phase plots (Figure 1a). In our model, the interaction that causes this change of behavior and that dominates the dynamics for energies around 13000−14000 is the Fermi coupling between the elementary modes *m* and *b* in the ratio 2:1. In this coupling, the new angle $\psi_m$ moves with average speed zero, i.e., the original modes *m* and *b* become locked. Accordingly, the skeleton element of this motion is a periodic orbit B running in the $\psi_n$ direction, and therefore, its average speed in the $\psi_m$ direction is zero. For some energies, it is stable and has a small KAM island around it; for other energies, it is unstable. Figure 3 shows the classical dynamics for energy 13184, the energy of quantum state 24. Part a shows a Poincare map, part b shows the periodic orbit B, and parts c−e show the motion in displacement space lifted from orbit B.

In the Poincare map, we see primary tori for large values of $J_m$ and a large chaotic sea for smaller values of $J_m$. Embedded in the large chaotic sea is a KAM island of moderate size. Its center represents the periodic orbit B shown in Figure 3b. The island is too small to carry states according to the EBK method, but the orbit B has a large influence on the motion in the chaotic sea and, thereby, has an influence on a large sequence of quantum states.

According to the dominance of the *m*−*b*−*b* Fermi resonance, the lifted motion in the *m*−*b* local-mode plane is locked and confined to a U-shaped strip because, in one period of motion, only the U has two sweeps of the *m* local mode for one sweep of the *b*. The motion in the *n* direction is uncoupled and independent, as seen from the fact that the motion in the *n* direction is almost a pure rotor on the configuration torus. A rotor in angle space is a free oscillator, here local, in the original coordinates. From Figure 1a, we see how the density crests in quantum states 19, 24, and 28 follow the classical orbit B. All density is concentrated along the orbit B. In this sense, we call such states the zeroth transversal excitation along orbit B and give them the transverse quantum number $t = 0$. The phase advance along the crest of density of these states for one complete loop in the $\psi_n$ direction is an integer multiple of $2\pi$, which we call the longitudinal excitation number *l*. In this sense, state 19 is the zeroth longitudinal excitation of orbit B, state 24 is the first longitudinal excitation, etc. In state 15, the density has a nodal line along orbit B and two crests on the two sides.

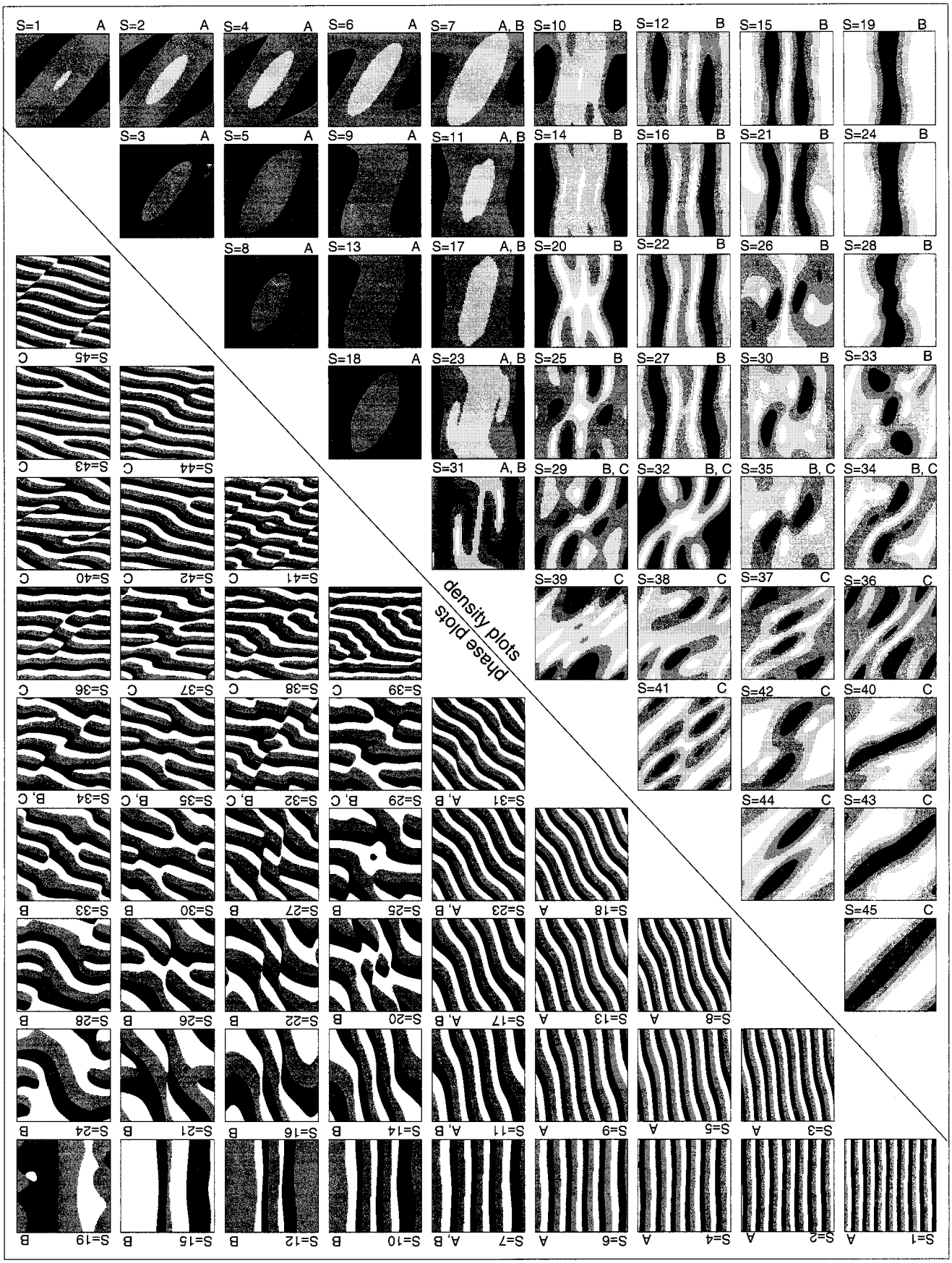
S=1 A
S=2 A
S=4 A
S=6 A
S=7 A, B
S=10 B
S=12 B
S=15 B
S=19 B
S=3 A
S=5 A
S=9 A
S=11 A, B
S=14 B
S=16 B
S=21 B
S=24 B
S=8 A
S=13 A
S=17 A, B
S=20 B
S=22 B
S=26 B
S=28 B
S=45 C
S=18 A
S=23 A, B
S=25 B
S=27 B
S=30 B
S=33 B
S=43 C
S=44 C
S=31 A, B
S=29 B, C
S=32 B, C
S=35 B, C
S=34 B, C
S=40 C
S=42 C
S=41 C
S=39 C
S=38 C
S=37 C
S=36 C
S=36 C
S=37 C
S=38 C
S=39 C
S=34 B, C
S=35 B, C
S=32 B, C
S=29 B, C
S=31 A, B
S=33 B
S=30 B
S=27 B
S=25 B
S=23 A, B
S=18 A
S=28 B
S=26 B
S=22 B
S=20 B
S=17 A, B
S=13 A
S=8 A
S=24 B
S=21 B
S=16 B
S=14 B
S=11 A, B
S=9 A
S=5 A
S=3 A
S=19 B
S=15 B
S=12 B
S=10 B
S=7 A, B
S=6 A
S=4 A
S=2 A
S=1 A
density plots
phase plots

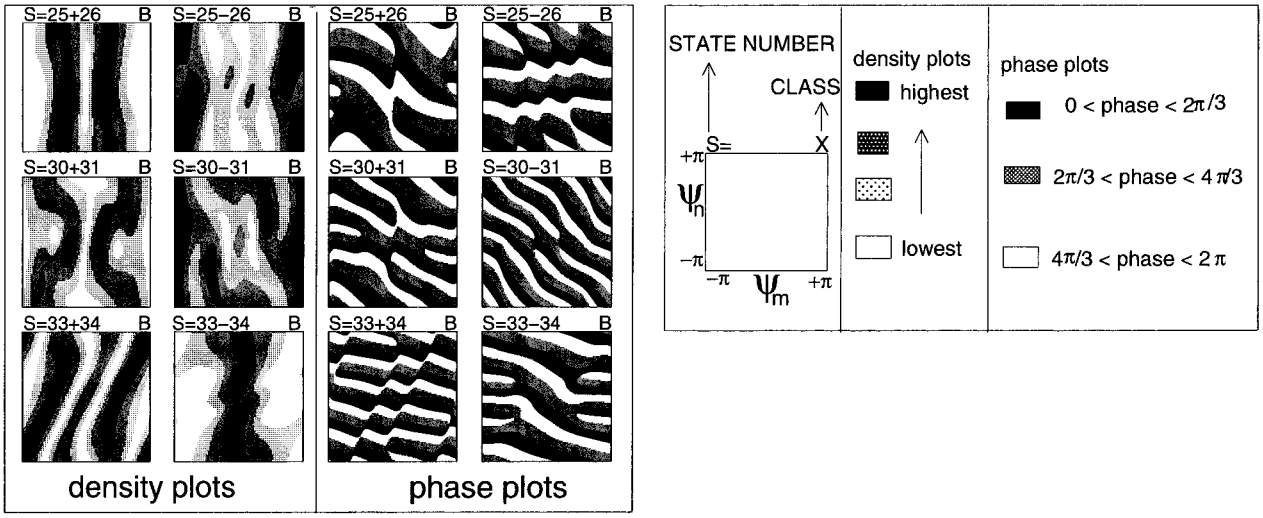


**Figure 1.** (a) Mercator plots of density and phase for all 45 states of polyad 8 in the reduced configuration space. (b) Mercator plots of density and phase for the symmetric and antisymmetric linear combinations of the pairs (25, 26), (30, 31), and (33, 34) of eigenstates. (c) Key for parts a and b.

We call such a structure the first transversal excitation of orbit B and give it quantum number $t = 1$. We also can identify various states as combined transversal and longitudinal excitations along orbit B. They are compiled in Table 1 where the quantum numbers $t$ and $l$ are given.

For energies around 12500, in the parts of the chaotic sea close to the remnants of the primary torus layer, the general trajectory shows a behavior similar to that inside of the primary torus region. In the rest of the chaotic sea, the general dynamics is heavily influenced by the periodic orbit B. With increasing energy, the relative importance of the primary torus zone decreases, and the relative importance of the periodic orbit B increases. The transition is rather smooth. Accordingly, in this transition region, we expect quantum states to show a smooth transition from the continuously deformed basis state structure, class A, to a structure resembling the flow along the orbit B. In this sense, the sequence of states 7, 11, 17, 23 can be classified using the phase diagrams (Figure 1a) as belonging to class A. However, if we chose to focus on density diagrams of these states, they resemble class B to their right in Figure 1a. As in class B, $l$ would come from the phase diagrams and $t$, in principle, from the transverse node counted in the density diagrams. Continuing from the right, we would expect this column of four states to have $t = 4$. We actually do not see the nodal lines, but the figures shows that this column of four states is definitely transition between class A and B. For the states 10, 12, 15, 14, and 16, the phase function is a continuous deformation of a basis function. Accordingly, these states can also be classified alternatively as class A, even though it seems more natural on the basis of the intensity plot to put them into class B. In Table 1, we indicate all alternative classifications where the less natural ones are put into brackets. At first sight, states 25 and 26 do not fit well into class B, even though some structural elements look like class B. The cause for this difficulty seems to be a quantum effect that is an accidental degeneracy and a corresponding wave function mixing. Note, in Table 1, how close in energy states 25 and 26 are. In Figure 1b, we also show the symmetric and antisymmetric linear combinations, which is the rotation of the states that minimizes the interference between states 25 and 26. They fit perfectly into class B as states with quantum numbers $t = 3$, $l = 3$ and $t = 1$, $l = 2$, respectively. In Table 1, we do not assign states 25 and 26, but just below them, we place the disentangled states. Similarly, the pair of states 30 and 31 and the pair 33 and 34 are each atypical, and internally, the pairs are very close in energy, a sign that they have to be disentangled before they can be classified properly. Figure 1b shows that states 30 and 31 disentangle to two states of class B whose assignments is indicated in the Table 1. Similarly, states 33 and 34, which can be very roughly assigned as in the table, can be disentangled to give the results shown in Figure 1b and indicated in Table 1. Clearly, the antisymmetric combination of the states is a class B state with $t = 0$, and its phase diagram would say $l = 3$. The symmetric combination will be interpreted after class C is discussed.

The physical implications of $l$ and $t$ in the classical motions and wave function nodal structures in both reduced and full dimensions require more discussion. These quantum numbers clearly arise when the motion is restricted to a ring-shaped region that loops the configuration torus. This localization defines which modes are locked and which of the old quantum numbers no longer exist. The locking anticipates the shape in 3D of the wave function projected into the plane of the locked modes. The ring direction is the "free" direction, and the phase advance in this direction tells us the degree of excitation, $l$, of the free mode. If all of the resonances in the effective Hamiltonian but the coupled ones were now ignored and the effective measure of the amount of excitation in the ring direction could be specified by an effective polyad number $\tilde{P}$[13] obtained by subtracting from $P$ the term associated in its definition with the free motion, $P$ would then tell us the degree of excitation expected in the 2D coupled wave function. Observation of the trajectories in 2D of such states tells us that $t$ correlates with the average amount of transverse (to the ring) quasioscillating motion that accompanies the rotation about the ring. It quantizes to the transverse nodes in 2D and can be correlated with the number of the nodes transverse to the locked motion (here the U). $\tilde{P}$ reduced by an integer times $t$ then tell us the number of nodes in 3D (not in 2D, because in 3D, we have coupled oscillator motion that shows nodes, but in 2D, we have a rotor whose excitation shows only in the phase) along the locked motion. Of course, in our case of multiple resonances and chaos, the wave functions usually at best only suggest that the above underlying order exist. All of the problems of inspecting $ND$, $N > 2$, wave functions plus the chaos prevent

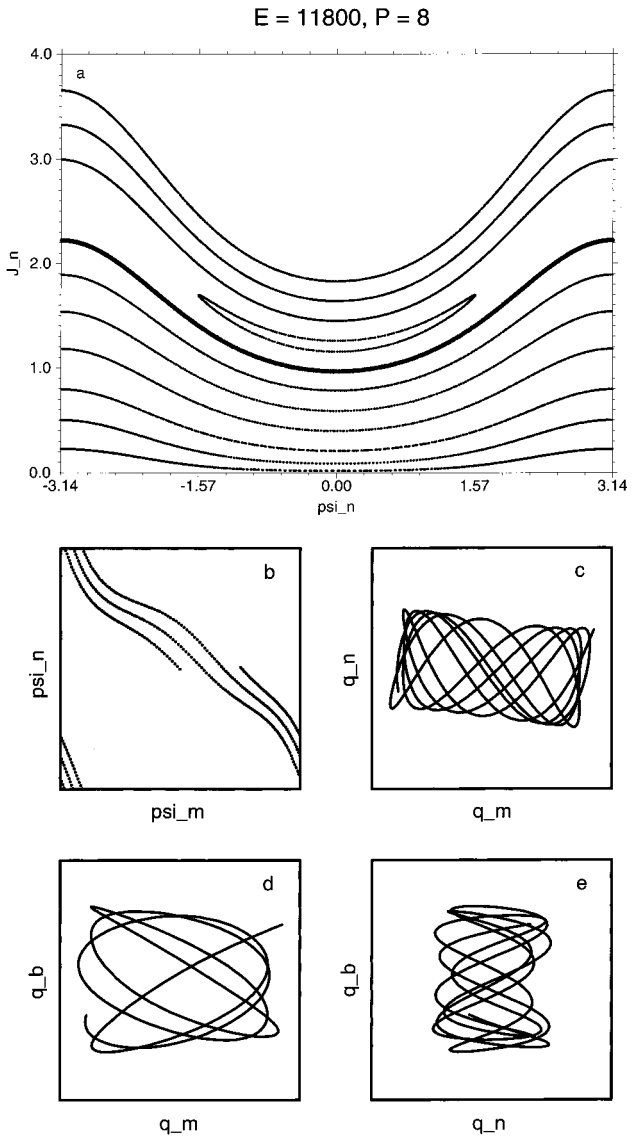


**Figure 2.** Classical dynamics at $E = 11800$ in polyad 8. Part a shows the Poincare plot in the plane $\psi_m = 0$ with negative orientation. The torus that carries quantum state 9 according to the EBK method is shown by the heavy line. Part b shows a trajectory segment on this quantizing torus projected into the configuration space. Parts c−e show the lift of the trajectory from part b into the displacement space, part c is the projection into the $m-n$ plane, part d is the projection into the $m-b$ plane, and part e is the projection into the $n-b$ plane. The frame boundaries in part b are $-\pi$ and $+\pi$, the frame boundaries of $q_m$ and of $q_n$ are $-3$ and $+3$, and the frame boundaries of $q_b$ are $-4$ and $+4$.

the clear observation of the ideal case, which is why we work in reduced space in the first place.

**3.3. Class C.** For still higher energy around 14000, the couplings between modes *m* and *n* take over and confine the accessible part of configuration space to a strip running in the diagonal direction. In phase space, the flow runs inside an imaginary guiding tube projecting onto this diagonal strip. Inside the tube, we find the period-one trajectories C1a, C1b, and C2 acting as guiding centers for the whole tube. The orbits C1a and C1b are symmetry images of each other; therefore, we can consider them as one periodic orbit C1. All of them have loop numbers 1 and 1, respectively, along the two fundamental cycles of the toroidal configuration space. Because periodic orbits C1 and C2 have different loop numbers than periodic orbit B, the transition from behavior dominated by orbit B into behavior dominated by orbits C1 and C2 cannot be as smooth as the transition between the behavior of classes A and B. Therefore, it is easier first to describe the behavior at the highest energies and then to describe the transitional region around energy

**TABLE 1: Classification and Assignment of All States of Polyad 8**[a]

| number | energy | class | EBK | *l* | *t* | *m* | *n* |
|---|---|---|---|---|---|---|---|
| 1 | 8931 | A | yes | − | − | 8 | 0 |
| 2 | 9845 | A | yes | − | − | 7 | 0 |
| 3 | 10485 | A | yes | − | − | 7 | 1 |
| 4 | 10614 | A | yes | − | − | 6 | 0 |
| 5 | 11216 | A | yes | − | − | 6 | 1 |
| 6 | 11236 | A | yes | − | − | 5 | 0 |
| 7 | 11704 | A | yes | − | − | 4 | 0 |
| | | (B) | no | 0 | 4 | − | 0 |
| 8 | 11779 | A | yes | − | − | 6 | 2 |
| 9 | 11800 | A | yes | − | − | 5 | 1 |
| 10 | 12010 | B | no | 0 | 3 | − | 0 |
| | | (A) | no | − | − | 3 | 0 |
| 11 | 12226 | A | yes | − | − | 4 | 1 |
| | | (B) | no | 1 | 4 | − | 1 |
| 12 | 12244 | B | no | 0 | 2 | − | 0 |
| | | (A) | no | − | − | 2 | 0 |
| 13 | 12325 | A | yes | − | − | 5 | 2 |
| 14 | 12471 | B | no | 1 | 3 | − | 1 |
| | | (A) | no | − | − | 3 | 1 |
| 15 | 12521 | B | no | 0 | 1 | − | 0 |
| 16 | 12656 | B | no | 1 | 2 | − | 1 |
| | | (A) | no | − | − | 2 | 1 |
| 17 | 12712 | A | yes | − | − | 4 | 2 |
| | | (B) | no | 2 | 4 | − | 2 |
| 18 | 12812 | A | yes | − | − | 5 | 3 |
| 19 | 12838 | B | no | 0 | 0 | − | 0 |
| 20 | 12884 | B | no | 2 | 3 | − | 2 |
| 21 | 12902 | B | no | 1 | 1 | − | 1 |
| 22 | 13031 | B | no | 2 | 2 | − | 2 |
| 23 | 13163 | A | yes | − | − | 4 | 3 |
| | | (B) | no | 3 | 4 | − | 3 |
| 24 | 13184 | B | no | 1 | 0 | − | 1 |
| 25 | 13233 | − | no | − | − | − | − |
| 26 | 13256 | − | no | − | − | − | − |
| 25 + 26 | 13245 | B | no | 2 | 1 | − | 2 |
| 25 − 26 | 13245 | B | no | 3 | 3 | − | 3 |
| 27 | 13379 | B | no | 3 | 2 | − | 3 |
| 28 | 13488 | B | no | 2 | 0 | − | 2 |
| 29 | 13527 | B | no | 4 | 3 | − | 4 |
| | | (C) | no | 4 | 1 | − | − |
| 30 | 13569 | (B) | no | 3 | 1 | − | 1 |
| 31 | 13579 | (A) | yes | − | − | 4 | 4 |
| 30 + 31 | 13574 | B | no | 3 | 1 | − | 3 |
| 30 − 31 | 13574 | B | no | 4 | 4 | − | 4 |
| | | (A) | yes | − | − | 4 | 4 |
| 32 | 13689 | B | no | 4 | 2 | − | 4 |
| | | (C) | no | 5 | 2 | − | − |
| 33 | 13752 | (B) | no | 3 | 0 | − | 3 |
| 34 | 13785 | (C) | no | 5 | 1 | − | − |
| 33 + 34 | 13763 | B | no | 5 | 2 | − | 5 |
| 33 − 34 | 13763 | B | no | 3 | 0 | − | 3 |
| 35 | 13848 | B | no | 4 | 1 | − | 4 |
| 36 | 13900 | C | no | 6 | 2 | − | − |
| 37 | 13985 | C | no | 6 | 1 | − | − |
| 38 | 14023 | C | no | 7 | 2 | − | − |
| 39 | 14055 | C | no | 8 | 3 | − | − |
| 40 | 14086 | C | no | 6 | 0 | − | − |
| 41 | 14130 | C | no | 8 | 2 | − | − |
| 42 | 14211 | C | no | 7 | 1 | − | − |
| 43 | 14330 | C | no | 7 | 0 | − | − |
| 44 | 14383 | C | no | 8 | 1 | − | − |
| 45 | 14540 | C | no | 8 | 0 | − | − |

[a] The first column gives the number of the states ordered by increasing energy. The second column gives the value of the energy in $cm^{-1}$. The third column gives the class to which the state is assigned. Column 4 indicates whether classification and quantum numbers are provided by the EBK method. Columns 5 and 6 give longitudinal and transverse quantum numbers *l* and *t*, respectively, for states of classes B and C. Columns 7 and 8 give quantum numbers *m* and *n*, respectively, of the basic modes for states of class A. Because, for states of class B, the longitudinal motion runs into the *n* direction, the longitudinal quantum number can also be interpreted as the quantum number of this local mode and is repeated in the corresponding column. For many states, alternative classifications are possible. Then, we give first the most natural or obvious classification (in particular that obtained from the EBK method) and give in parentheses on the line below the alternative classification. For states 25, 26, 30, 31, 33, and 34, we have also used the untangling described in the main text to determine the classification.

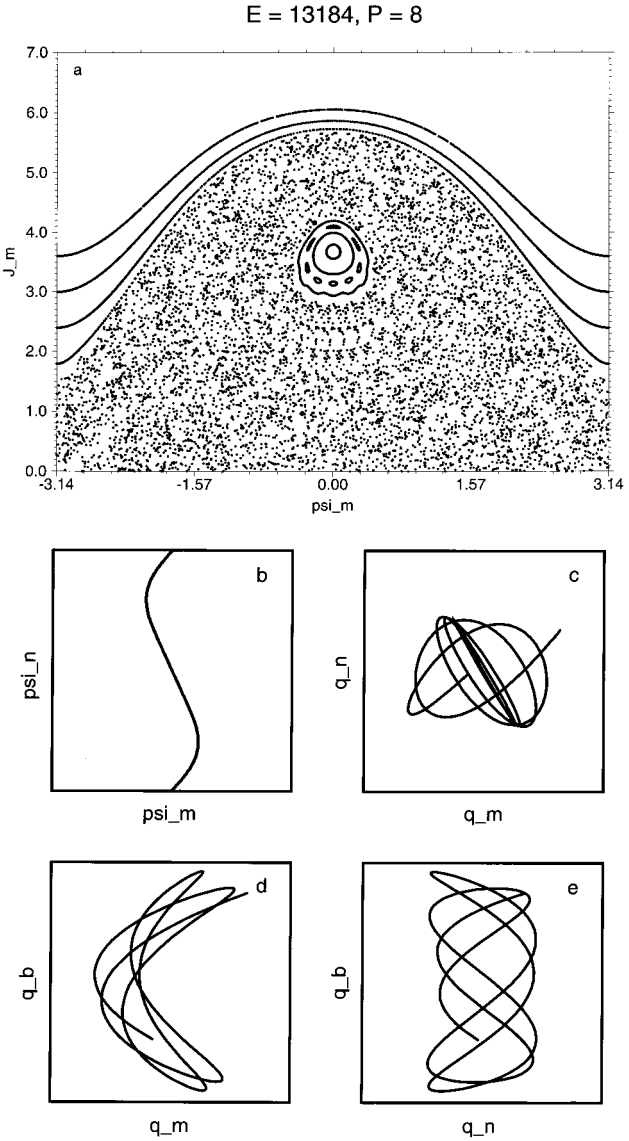


**Figure 3.** Classical dynamics at $E = 13184$ in polyad 8. Part a gives the Poincare section in $\psi_m = 0$ with negative orientation. Part b shows the periodic orbit B in reduced configuration space. Parts c−e show the lift of the orbit B. Otherwise, it is constructed like Figure 2.

13500−14000 later. For energies above 14100, where the orbit B has disappeared and where only classical motion in the diagonal direction is possible, the quantum states show a very clear alignment in the diagonal direction. Clearly, here, $<\psi_a> = <\psi_b>$, and therefore, $\dot{\psi}_a = \dot{\psi}_b$, and by eq 6, $\omega_n = \omega_m$; hence, the local modes phase lock.

In Figure 4 , we show the classical dynamics at energy 14540 which is the energy of the highest quantum state. Part a shows the Poincare section, part b shows orbit C1, parts c−e show the lift of orbit C1, part f shows orbit C2 and parts g−i show the lift of orbit C2. In part b, we show both symmetry-related copies of orbit C1. In parts c−e, we show the lift of just one of the two copies; the other produces the same lift because of symmetry. In the Poincare plot, we do not detect any KAM island of reasonable size; the dynamics is close to completely chaotic. The dynamics is dominated by $m-n$ coupling, which leads to the highly correlated motion in the $(\psi_m, \psi_n)$ plane, which is an oscillation around the diagonal motion. It is easy to imagine how the orbits C1a, C1b, and C2 together guide all of the flow in the diagonal direction. The mode $b$ is free and independent and keeps its local-mode character. In the plot of

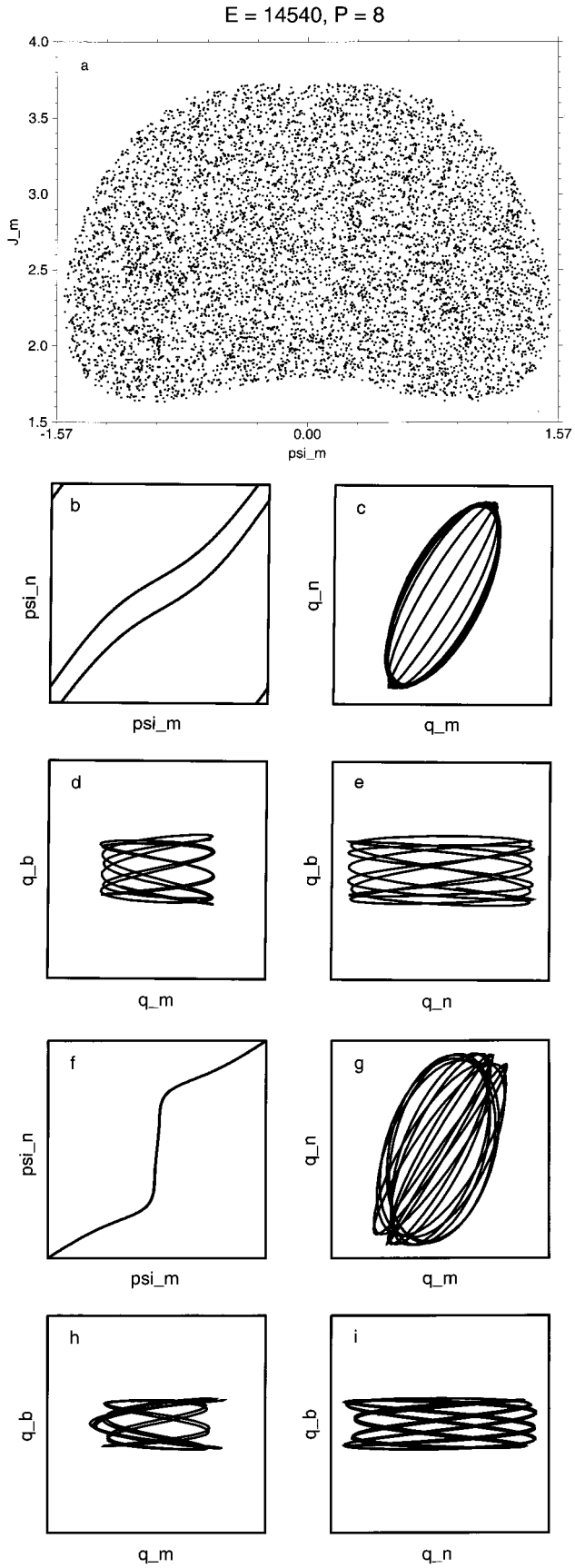


**Figure 4.** Classical dynamics at $E = 14540$ in polyad 8. Part a gives the Poincare section in $\psi_n = 0$ with positive orientation. Part b shows the periodic orbits C1a and C1b in reduced configuration space. Parts c−e show the lift of orbit C1. Part f shows the periodic orbit C2 in reduced configuration space. Parts g−i show the lift of orbit C2. Otherwise, it is constructed like Figure 2.

the wave function for state 45, we see a clear confinement of the density to a strip in the diagonal direction. The transverse excitation number is $t = 0$. The phase advance along the density crest is $8 \times 2\pi$, which shows, because $P = 8$, that all excitation is in the perfectly coupled $m-n$ motion. Our model formulated in abstract modes does not indicate the absolute or relative phases of the motion of the atoms in the molecule. This is seen from the absence of a phase $\alpha_k$ in the exponential in eq 9. Hence, we cannot determine whether the coupled motion is quasiantisymmetric ($\alpha_m - \alpha_n = \pi$ and the guiding periodic orbit along the negatively sloped direction in the $q_m$ versus $q_n$ plane); quasisymmetric ($\alpha_m - \alpha_n = 0$ and a periodic orbit in positively sloped direction); or even an intermediate trajectory as a negatively sloped (major axis of) ellipse, a circle, or a positively sloped ellipse as $\alpha_m - \alpha_n$ varies from $\pi$ to zero. To determine where we are in this "spectrum of motions", we must therefore determine the relative phase. In fact, in Figure 4c and g, because we did not know the phases, we arbitrarily set all phases to zero. To settle this issue, we seek a 3D periodic orbit or near-periodic orbit associated with this state to observe its qualitative nature. In practice, because this is the highest state in the polyad and because lower polyads have qualitatively the same type of state, as we see for state 45 in Figure 1a, we could work at lower total excitation $P$, and finding such a trajectory would not be difficult. In this case, the search is made easy by the work of ref 4, where the 3D periodic orbit associated with state 45 has been located and shown to be quasiantisymmetric i.e., negative slope. Hence, for us, it has a relative phase of $\pi$.

In comparison to state 45, in state 43, the longitudinal excitation has decreased to 7, which indicates that one quantum is taken out of the $m-n$ motion and converted into $b$ excitation. This is consistent with what one sees in comparing how the important number representation basis functions change in the 3D representations of states 45 and 43. For comparison, in state 44, the longitudinal excitation is still eight, whereas there is one quantum of transverse excitation. This means that most excitation is still in the combined $m-n$ motion, but one of the quanta has gone into the out-of-phase motion. To see this, we observe in Figure 1a that the excitation of the transverse direction in the ($\psi_m$, $\psi_n$) plane causes a broadening of the wave function transverse to the positively sloped line, which we now know should be rotated to negative slope, and that it is the quasiantisymmetric motion. Classically, plots such as those shown in Figure 4b and 4f lead us to believe that transverse broadening causes the trajectory in this plane to fluctuate even more widely, but with a mean of zero, about a line of positive slope. This, in turn, causes in the ($q_m$, $q_n$) lifted plane, as suggested by Figure 4c and 4g (recall that we now know the ellipse should be rotated to the negative slope direction), an elliptical shape that, on average, has a larger minor axis. It follows that this introduces more elements of symmetrical (which is the motion transverse to the quasiantisymmetrical) motion. Hence, in a sense, the transverse excitation is that of a quasisymmetric stretch mode. All quantum states based on this diagonal motion are classified as class C, and their corresponding longitudinal and transverse excitation numbers are given in Table 1.

**3.4. Transitional States—The Importance of Overshadowing.** There remain a few states that are more difficult to interpret from wave function inspection; they are states 29, 32, 34 (also after demixing with 33), 36, and 37. They all lie in the transition region in phase space between classes B and C. The difficulty comes from the coexistence of the organizational elements for classes B and C, i.e., the periodic orbits B and $C_1$, $C_2$. They have winding numbers (0, 1) and (1, 1) on the toroidal configuration space, respectively. As a consequence, an infinity of other periodic orbits having various winding numbers $l_m$ and $l_n$ on the configuration torus exist, where the ratio between $l_m$ and $l_n$ can be any rational number between 0 and 1. Some, such as those with loop numbers $l_m = 1$, $l_n = 2$ and $l_m = 2$, $l_n = 3$, are sufficiently important to have an influence on a few quantum states and to impose a corresponding winding ratio in the path following the density crest of such functions. In the spirit of higher-order perturbation theory, these orbits can be thought of as created by the corresponding multiple combinations of the interaction terms in the Hamiltonian. Correspondingly, some quantum states should show a mixture of features belonging to classes B and C. We now briefly describe possible classifications of these states.

*State 29.* This state can be interpreted as a perturbed class B state with quantum numbers $l = 4$, $t = 3$ or even as a class C state with $l = 4$, $t = 1$. At the same time, it shows a pattern of winding ratio 1:2 (slope), indicating that the motion upon which this state is quantized is a trajectory that loops once around about periodic orbit B with winding ratio 0:1 for each time it loops about the periodic orbits of type C with winding ratio 1:1. This would give a net $n$:$m$ winding ratio of 1:2 and could have features of both the class B and class C states.

The appearance of longer resonant periodic orbits as combinations of the shortest periodic orbits as templates demonstrates the idea of overshadowing. Typically, as the interaction terms become more important, one first recognizes the basic (shortest, simplest, template) orbits and, with increasing effect of the coupling, also some combinational orbits. In our case, the combinational orbit observed, the one with winding ratio 1:2, can be described as a one plus one composition of the basic orbit of class B having winding ratio of 0:1 with the basic orbit of class C having a winding ratio of 1:1.

*State 32.* This state can be interpreted as a perturbed class B state with quantum numbers $l = 4$, $t = 2$ or even a C-type state with $l = 5$, $t = 2$.

*State 34.* Before demixing with state 33, this state shows a 1:2 winding ratio and can be interpreted as a perturbed state of class C with $l = 5$, $t = 1$. After demixing, because of accidental degeneracy, Figure 1b shows that it can be considered as a class B state with $l = 5$ and $t = 2$ or, better, as a state with slope $^1/_3$, indicating a 1:3 winding ratio that loops around the 0:1 B-type periodic orbit twice for every time it loops the 1:1 C-type periodic orbit.

*State 36.* This state shows a 2:3 winding ratio in its density crest. It can be interpreted as a perturbed state of class C with $l = 6$, $t = 2$ or a motion that loops the C 1:1-type periodic orbit twice for each looping of the B-type 0:1 state.

*State 37.* This state is the perturbed state of class C with quantum numbers $l = 6$, $t = 1$.

For higher polyads, one can expect ladders of states built on periodic orbits with winding ratios such as 1:3 and 2:3.

Also, a few other states with lower energy that we have already assigned to class B can alternatively be interpreted as highly perturbed states of class C. See the alternative assignments given in Table 1.

In the classification and assignments of the highly perturbed states, we have also taken account of the energy spacings in various ladders of states to determine whether they appear to fit those of the particular sequence.

This multiple classical assignment is the dynamic generalization and explanation of the fact that, in quantum mechanics, significant weights, often greater than 50%,[14] can be found on

a single configuration for each of two different basis sets usually formed from oscillator functions along orthogonal coordinate systems (e.g., normal or local). Clearly, the dynamic explanation is more powerful, as wave functions, or more precisely packets, follow classical organizing structures rather than coordinates chosen for convenience. The same dynamic effective forces that confine trajectories defining organizing structures also confine the wave packets which when Fourier transformed, give similarly confined wave functions.[15] Several comments are in order. First, note that each class of states can be viewed as a ladder of states with some shared rungs. The ladders overlap in energy so that states of different dynamic types interleave.

Second, in experimental and theoretical calculations,[1,3] no local-mode resonance states exist. We obtain them because no continuum sink is in the spectroscopic Hamiltonian and no decay is possible. Polyad 8 is made completely of resonances, so only class B and C and mixed states actually exist. The reason for this is that the local modes are decoupled modes, and therefore, the D−C motion, which points to the exit channel leading to D + CO, has no restraint on its tendency "to head out the door", which, in turn, means that no resonance exists. The other states that are resonances exist because the DCO motion is restrained by the resonant coupling in the spectroscopic Hamiltonian. It is not clear that anything can be said on the basis of the dynamics about the magnitude of the lifetimes of states in class B as opposed to class C. The absence of states with $n-b-b$ Fermi-resonant coupling is no mystery. Simply put, we see no region of phase space that corresponds to $n-b-b$ that is big enough to accommodate the semiclassical volume of such states. The region we do see is too small to hold states, and nearby trajectories are not influenced by it.

## 4. Conclusions

At this point, a significant practical point can be made about the analysis. The analysis as done in this paper reveals the types of classical dynamics exhibited by the molecule and then uses the ideas about classical trajectories and wave functions following organizing structures to associate states with dynamics and appropriate assignments. Now, if one is interested not in insights into classical dynamics but rather in molecular motions and the assignment, it would be possible to obtain most, albeit not all, of this latter information without carrying out much dynamics. For example, the class B states all lie on a vertical intensity strip, and the quantum numbers come from quantum phase and node counts. One would not know if the organizing structure was a periodic orbit or a torus or several periodic orbits running parallel to $\psi_n$ in a region where $<\dot{\psi}_m> = 0$, but one could infer $<\dot{\psi}_m> = 0$ from wave function localization, and from there, one could infer the U-shaped motion in the $m-b$ local-mode plane and the nearly uncoupled motion of the local mode in the other two planes. Clearly, here, one uses the principles of nonlinear dynamics and semiclassical mechanics without calculating trajectories. Of course, the full method is superior, but for those unskilled in the art of investigating phase space or for those who want rapid qualitative insights, the latter approach will yield much of the desired knowledge without any significant calculations other than producing the phase and intensity pictures using the expansion coefficients of the wave functions obtained during the fit of the Hamiltonian to the experimental spectra.

A method for extracting the dynamics and assignments of the highly excited vibrational levels of DCO directly from spectra has been presented and applied successfully. DCO, because of its multiple resonant pattern, previously had not been fully and meaningfully assigned, even though 3D wave functions and periodic orbits in the phase space of this 3D system were known. The advantage of the present type of analysis is made apparent by the completeness of the physically meaningful assignment and the detailed unveiling of the underlying, often complex, dynamics.

**Acknowledgment.** C.J. is thankful to H.S.T. and the University of Southern California for hospitality during his research visit in November 2000. H.S.T. acknowledges support from the U.S. Department of Energy (DE-FG03-01ER1547). In Mexico, C.J. was supported by CONACyT (33773-E). H.S.T and E.A. thank the International Science Center at UNAM in Cuernevaca for its support and hospitality during their visit to Mexico.

## References and Notes

(1) Troellsch, A.; Temps, F. *Z. Phys. Chem.* **2001**, *215*, 207.
(2) Stöck, C.; Li, X.; Keller, H. M.; Schinke, R.; Temps, F. *J. Chem. Phys.* **1997**, *106*, 5333.
(3) Keller, H. M.; Stumpf, M.; Schröder, T.; Stök, C. *J. Chem. Phys.* **1997**, *106*, 5359.
(4) Stamatiadis, S.; Farantos, S. C.; Keller H. M.; Schinke, R. *Chem. Phys. Lett.* **1999**, *311*, 241.
(5) Kellman, M. E. *J. Chem. Phys.* **1990**, *93*, 6630.
(6) Fried, L. E.; Ezra, G. S. *J. Chem. Phys.* **1987**, *86*, 6270.
(7) Jacobson, M. P.; Jung, C.; Taylor, H. S.; Field, R. W. *J. Chem. Phys.* **1999**, *111*, 600.
(8) Jung, C.; Taylor, H. S.; Jacobson, M. P. *J. Phys. Chem. A* **2001**, *105*, 681.
(9) Jung, C.; Ziemniak, E.; Taylor, H. S. *J. Chem. Phys.* **2001**, *115*, 2499.
(10) Waalkens, H.; Jung, C.; Taylor, H. S. *J. Phys. Chem. A* **2002**, *106*, 911.
(11) Sibert, E. L., III; McKoy, A. B. *J. Chem. Phys.* **1996**, *105*, 469.
(12) Gutzwiller, M. C. *Chaos in Classical and Quantum Mechanics*; Springer: New York, 1990.
(13) Lu, Z. M.; Kellman, M. E. *J. Chem. Phys.* **1997**, *107*, 1.
(14) Hose, G.; Taylor, H. S. *Phys. Rev. Lett.* **1983**, *51*, 947.
(15) Hose, G.; Taylor H. S.; Bai, Y. Y. *J. Chem. Phys.* **1984**, 80, 4363.